Dalton Transactions

PAPER

View Article Online
View Journal



Cite this: DOI: 10.1039/c7dt01699a



# Radical reactions of diamine bis(phenolate) vanadium(III) complexes. Solid state binding of $O_2$ to form a vanadium(V) peroxo complex†

Sónia Barroso, [a] Ana M. Coelho,[a] Pedro Adão, [a] Maria José Calhorda [b] and Ana M. Martins *[a]

$[VCl_3(THF)_3]$ reacted with the sodium salt of a tripodal diamine bisphenolate ligand precursor $Na_2L2$ to give a paramagnetic $d^2$ complex [V(L2)Cl] (**2**). The reaction of **2** with oxygen is strongly dependent on the experimental conditions, affording [VO(L2)Cl] (**6**) or $[V(\eta^2\text{-}O_2)(L2)Cl]$ (**7**). The formation of **7** involves the direct addition of $O_2$ to V(III) in the solid state with oxidation to V(V) without significantly disturbing the structure of **2**. DFT calculations showed that compound **7** is an intermediate in the formation of **6** from **2**. The reaction involves the cleavage of the $\eta^1$-O–O bond in a proposed dimeric species. The overall reaction of 2 moles of vanadium(III), complex **2**, and one mole of $O_2$ to yield two moles of product **6** is a favourable process with $\Delta G_{298} = -38.3$ kcal mol$^{-1}$. **7** is the first non-oxido peroxidovanadium(V) complex obtained directly from the reaction of a crystal and the second example of a structurally characterized complex of that type. Reactions of V(L1)Cl (**1**) and V(L2)Cl (**2**) with one equivalent of the nitroxyl radical TEMPO in toluene also result in the formation of oxido V(V) complexes, VO(L1)Cl (**5**) and VO(L2)Cl (**6**). The reaction of $VO(O^iPr)_3$ with $Na_2L2$ afforded [VO(L2)($O^i$Pr)] (**8**) in high yield. A major isomer having the V=O moiety in the equatorial plane was characterised by X-ray diffraction although solution NMR data showed the presence of a minor species with the oxido ligand *trans* to the tripodal nitrogen, as in **6**. Complexes **6** and **8** are very active and selective sulfoxidation catalysts of thioanisole, but no enantiomeric excess was obtained.

Received 10th May 2017,
Accepted 30th June 2017

DOI: 10.1039/c7dt01699a

rsc.li/dalton

## Introduction

Vanadium plays an important role in biological systems, being present in the active sites of some haloperoxidases and nitrogenases.[1–6] The coordination chemistry of vanadium has therefore received considerable attention and led to relevant applications, in medicine,[1] mostly as an insulin mimetic, and as a catalyst in oxidation and oxo transfer reactions.[7–9]

Models of enzyme active centers or as oxidation/oxo transfer catalysts based on vanadium and molybdenum which are very relevant biological metals have been reported.[10,11] In the case of vanadium, such models often include oxidovanadium(IV) and -(V) fragments supported by N/O donor ligands with several architectures.[3,4,7,9,12,13] Significant effort has been made towards the development of asymmetric oxidation green catalysts, using $H_2O_2$ or $O_2$, though very few highly enantioselective oxidations in water have been reported.[14] The interaction of $O_2$ or $H_2O_2$ with metal complexes leading to well-defined species often lacks selectivity due to uncontrolled secondary reactions, being therefore a relevant issue toward the solution of this problem.

The chemistry of vanadium(III), however, is much less explored.[15–19] Despite the identification of V(III) and non-oxido V(IV) species in many enzymes, such as vanadium nitrogenase, the extreme susceptibility to the oxidation of vanadium(III) complexes and their di-radical nature have made the study of such species extremely challenging.

Our recent advances in the chemistry of transition metal complexes (Ti, Zr, V, Mo, W) coordinated to tripodal diamine bis(phenolate) ligands ($N_2O_2$)[20–24] showed that V(III) derivatives provided a convenient entry in the chemistry of oxido vanadium(V) complexes, which exhibited remarkable activity and selectivity in sulfoxidation catalysis. Despite our successful efforts to synthesise a chiral $N_2O_2$ ligand, no enantioselectivity could be achieved by the resulting complex in sulfoxidation catalysis and, as revealed by NMR studies,

[a]Centro de Química Estrutural, Instituto Superior Técnico, Universidade de Lisboa, Av. Rovisco Pais, 1049-001 Lisboa, Portugal. E-mail: ana.martins@ist.utl.pt
[b]Centro de Química e Bioquímica, DQB, Faculdade de Ciências, Universidade de Lisboa, Campo Grande, Ed. C8, 1749-016 Lisboa, Portugal

†Electronic supplementary information (ESI) available. CCDC 1536781–1536786. For ESI and crystallographic data in CIF or other electronic format see DOI: 10.1039/c7dt01699a

several species were present in solution upon addition of $H_2O_2$ to the catalyst precursors.[25] These studies on oxygen activation and sulfoxidation catalysis are followed in the present work. We demonstrate now that V(III) species react with molecular oxygen through a biradical process that forms an unusually rare non-oxido vanadium(V) peroxido complex, which rearranges to give a terminal V=O fragment. Relevant issues concerning the formation and stability of vanadium peroxido *vs.* vanadium oxido species are discussed on the basis of DFT calculations.

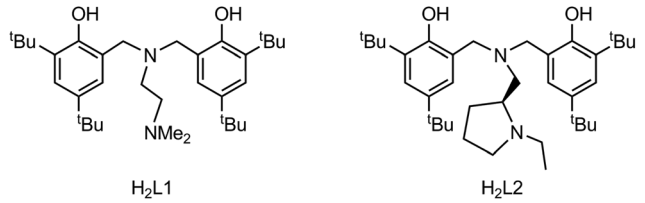


**Fig. 1** Tripodal diamine bis(phenolate) ligand precursors.

## Results and discussion

### Chemical studies

The vanadium complexes described here have as ancillary ligands diamine bis(phenolates) obtained from the $H_2L1$ and $H_2L2$ precursors displayed in Fig. 1.[26,27] The reaction sequences that led to the syntheses of all vanadium complexes described are depicted in Scheme 1.

$[VCl_3(THF)_3]$ was treated with 1 equivalent of the sodium derivative of $H_2L1$ forming [V(L1)Cl(THF)] (**1**).[25] The parallel reaction between $[VCl_3(THF)_3]$ and $Na_2L2$ led to the new [V(L2)Cl] complex (**2**) as a crystalline red solid in 63% yield

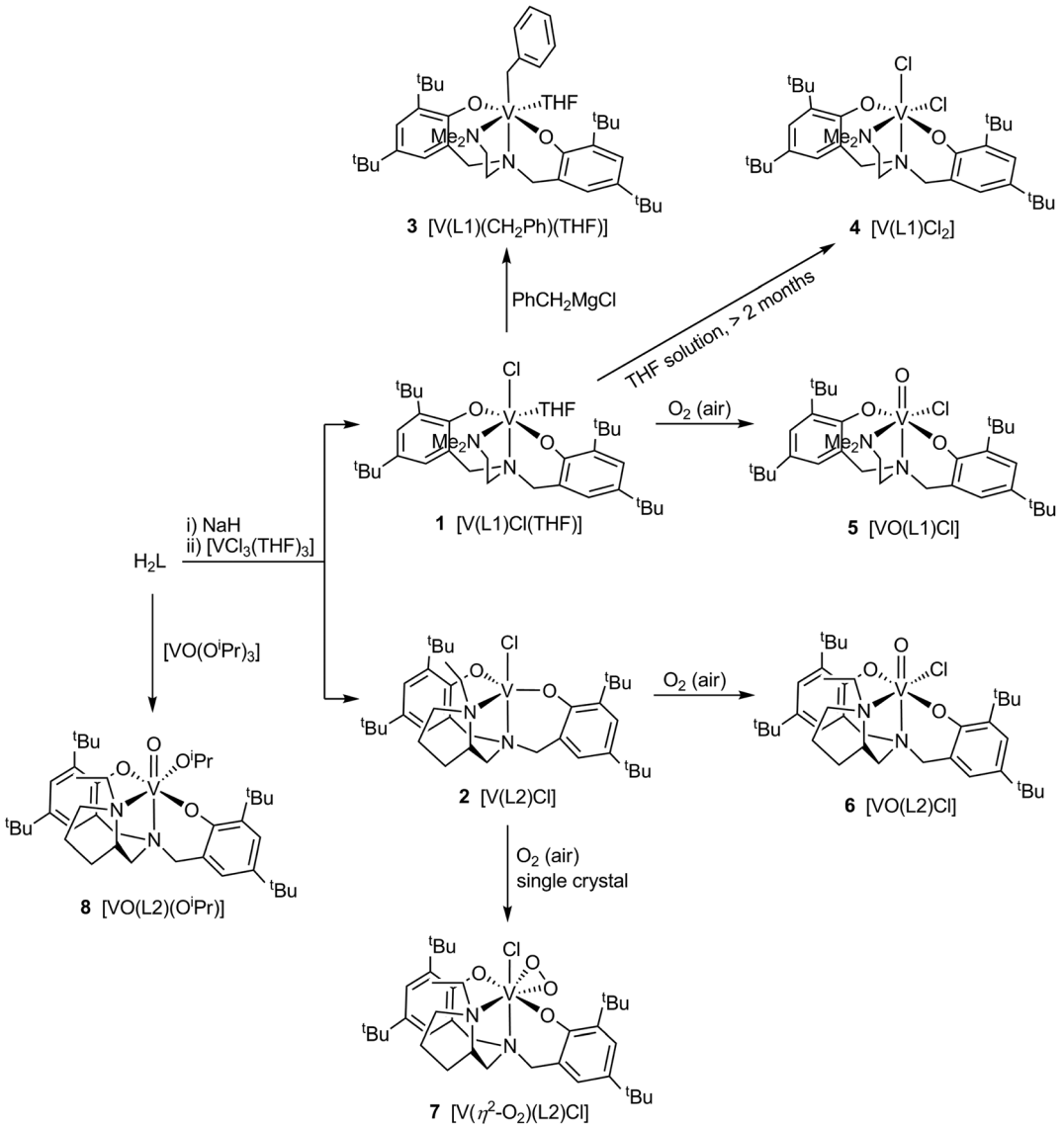


**Scheme 1** Reaction sequences for the syntheses of the vanadium complexes.

(Scheme 1). As expected for a paramagnetic $d^2$ species, the magnetic susceptibility of **2** was determined as $\mu_{eff}$ (18 °C) = 2.36$\mu_B$, very close to that of **1** ($\mu_{eff}$ (22 °C) = 2.45$\mu_B$).

The molecular structure of **2** was obtained by single crystal X-ray diffraction and is depicted in Fig. 2. Selected structural parameters are listed in Table 1. The compound crystallises from $Et_2O$ in the monoclinic system, space group $P2_1$, containing one molecule of **2** and one $Et_2O$ solvate molecule in the asymmetric unit. The penta-coordination geometry in **2** is best described as distorted trigonal bipyramidal with atoms O1, O2 and N2 defining the equatorial plane and atoms N1 and Cl1 occupying the axial positions. The lower coordination number of vanadium in **2** (by comparison with **1**) is probably imposed by the bulky and fairly rigid ethylpyrrolidine moiety that pushes the phenolate moieties back and forces the loss of THF. Indeed, the O1–V1–O2 angle in **2** (125.8(1)°) is much narrower that in **1** (165.58(2)°).[25]

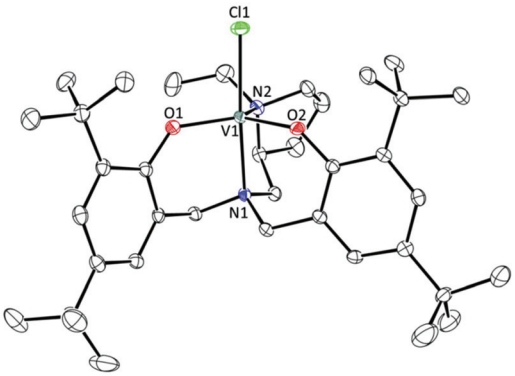


**Fig. 2** ORTEP-3 diagram of [V(L2)Cl] (**2**), using 40% probability level ellipsoids. Hydrogen atoms are omitted for clarity.

The 5-membered metallacycle defined by V1–N1–C1–C2–N2 displays a $\delta$ conformation with *S* configuration at the chiral centres N2 and C2. The V–N1 and V–N2 distances, 2.178(3) and 2.135(3) Å, respectively, are consistent with those in the few aminephenolate vanadium(III) complexes reported.[17,28] The V–$O_{phenolate}$ distances in **2** (1.862(2) and 1.859(2) Å) are smaller than in **1** (1.906(4) and 1.913(4) Å), indicating a more pronounced π-bonding character made possible by the lower coordination number, but agree well with the distances observed in the aminetrisphenolate vanadium(III) complex

**Table 1** Selected structural parameters for **2**, **3**, **4**, **6**, **7** and **8**(*1*)

| | **2** | **3** | **4** | **6** | **7** | **8**(*1*) |
|---|---|---|---|---|---|---|
| Distances (Å) | | | | | | |
| V(1)–N(1) | 2.178(3) | 2.259(2) | 2.214(3) | 2.319(3) | 2.25(2) | 2.249(4) |
| V(1)–N(2) | 2.135(3) | 2.231(2) | 2.230(3) | 2.273(4) | 2.30(2) | 2.464(4) |
| V(1)–O(1) | 1.862(2) | 1.937(2) | 1.789(2) | 1.843(3) | 1.83(2) | 1.898(3) |
| V(1)–O(2) | 1.859(2) | 1.929(2) | 1.783(2) | 1.838(4) | 1.76(1) | 1.913(3) |
| V(1)–X1[a] | 2.362(1) | 2.192(2) | 2.316(1) | 2.341(2) | 2.33(1) | |
| V(1)–X2[a] | | 2.181(2) | 2.335(1) | 1.597(3) | 1.78(2) | 1.772(3) |
| V(1)–O(4) | | | | | 1.85(1) | 1.589(3) |
| O3–O4 | | | | | 1.39(2) | |
| V(1)-eq. plane[b] | 0.133(1) | 0.159(1) | 0.152(1) | 0.240(1) | 0.284(8) | 0.210(1) |
| Angles (°) | | | | | | |
| O(1)–V(1)–O(2) | 125.8(1) | 165.4(1) | 169.4(1) | 163.0(1) | 169.4(6) | 161.0(1) |
| O(1)–V(1)–X2 | | 84.2(1) | 89.4(1) | 99.4(2) | 87.4(6) | 97.4(1) |
| O(1)–V(1)–O(4) | | | | | 93.5(6) | 95.1(1) |
| O(2)–V(1)–X2 | | 83.6(1) | 89.7(1) | 97.5(2) | 90.6(6) | 96.2(1) |
| O(2)–V(1)–O(4) | | | | | 92.3(6) | 93.4(1) |
| X2–V(1)–O(4) | | | | | 44.7(6) | 107.7(1) |
| O(1)–V(1)–N(1) | 89.0(1) | 85.1(1) | 82.9(1) | 80.2(2) | 87.8(5) | 78.7(1) |
| O(2)–V(1)–N(1) | 87.5(1) | 87.3(1) | 86.5(1) | 84.4(2) | 81.7(6) | 83.5(1) |
| X2–V(1)–N(1) | | 92.3(1) | 92.2(1) | 162.4(2) | 79.7(7) | 155.6(2) |
| O(4)–V(1)–N(1) | | | | | 124.3(7) | 96.7(2) |
| O(1)–V(1)–N(2) | 119.1(1) | 97.1(1) | 92.0(1) | 93.1(2) | 89.8(6) | 83.1(1) |
| O(2)–V(1)–N(2) | 113.7(1) | 93.7(1) | 87.6(1) | 90.0(2) | 88.0(6) | 85.9(1) |
| X2–V(1)–N(2) | | 171.2(1) | 172.7(1) | 86.8(2) | 156.6(6) | 81.3(1) |
| O(4)–V(1)–N(2) | | | | | 158.6(6) | 171.1(1) |
| N(1)–V(1)–N(2) | 81.2(1) | 79.2(1) | 80.8(1) | 75.6(1) | 77.0(6) | 74.4(1) |
| O(1)–V(1)–X1 | 95.5(1) | 94.2(1) | 94.7(1) | 86.3(1) | 94.7(4) | |
| O(2)–V(1)–X1 | 92.9(1) | 95.1(1) | 95.9(1) | 87.5(1) | 95.1(5) | |
| X2–V(1)–X1 | | 95.7(1) | 96.8(1) | 104.0(1) | 123.7(5) | |
| O(4)–V(1)–X1 | | | | | 79.0(5) | |
| N(1)–V(1)–X1 | 174.2(1) | 171.9(1) | 170.6(1) | 93.5(1) | 156.5(5) | |
| N(2)–V(1)–X1 | 93.3(1) | 92.9(1) | 90.2(1) | 169.1(1) | 79.7(5) | |
| $\theta$[c] | 111.6(1) | 154.6(1) | 160.6(2) | 125.1(1) | 117.3(7) | 109.7(1) |

[a] X1 = C(81) for **3** and Cl(1) for **2**, **4**, **6** and **7**; X2 = Cl(2) for **4** and O(3) for **3**, **6**, **7** and **8**. [b] The equatorial plane is defined by atoms O(1), O(2), N(2) and Y in **3**, **4**, **6**, **7** and **8** (Y = O(3), Cl(2), Cl(1), O(3) and O(4), respectively) and by atoms O1, O2 and N2 in **2**. [c] $\theta$ is the dihedral angle between the planes containing the phenolate rings.

$[V(N(CH_2\text{-}2\text{-}O\text{-}3,5\text{-}^tBu_2\text{-}C_6H_2)_3)(THF)]$[28] that also displays trigonal bipyramidal geometry.

The reaction of **1** with 1 equiv. of $PhCH_2MgCl$ afforded $[V(L1)(CH_2Ph)(THF)]$ (**3**) as a green crystalline solid in 82% yield. The magnetic moment of **3** at 25 °C is 2.57$\mu_B$, typical of $d^2$ V(III) complexes. The structure of **3** was further confirmed by X-ray diffraction analysis. Complex **3** (Fig. 3) crystallizes from $Et_2O$ in the monoclinic system, space group $P2/c$, with one molecule of **3** and one $Et_2O$ solvate molecule in the asymmetric unit. Selected structural parameters are listed in Table 1. The coordination geometry is distorted octahedral, as in the precursor **1**,[25] with the equatorial plane defined by atoms O1, O2 and N2 of the diaminebisphenolate L2 ligand and the atom O3 of the THF ligand, while the axial positions are occupied by the tripodal nitrogen N1 and the methylene carbon atom C81 of the benzyl ligand. The overall structural parameters of **3** agree well with those of **1**, despite the longer V–N and $V\text{–}O_{phenolate}$ bond distances observed in **3**. In particular, the V1–N1 distance is significantly elongated [2.260(2) Å *vs.* 2.193(5) Å], reflecting the *trans* influence of the benzyl ligand. The V–C bond distance [2.192(2) Å] is comparable to the one observed in $[V(acacen)(CH_2Ph)]$ [2.156(9) Å, acacen = *N*,*N*′-ethylanebis(acetylacetone iminato) dianion].[29]

When **1** was kept for periods of 2–3 months in solution, blue crystals of a vanadium(IV) dichloride species $[V(L1)Cl_2]$ (**4**) were formed. This product most likely results from a disproportionation reaction of the vanadium(III) complex **1**, through an intermediate dinuclear species having chloride bridges, which may arise upon THF dissociation from **1**. Related disproportionation processes were observed for titanium analogues for which the dissociation of a labile ligand, as THF, forms bridging chloride dimers that rearrange to stable Ti(IV) and unstable Ti(II) species.[20,22] The EPR spectrum of **4** in toluene displays symmetrical single lines ($g$ = 1.967) characteristic of vanadium(IV). The $g$ value is similar to the one observed for an analogous [V(L)Cl2] vanadium(IV) complex reported in the literature, with L carrying methyl rather than *tert*-butyl substituents in the phenolates.[30] An EPR analysis of the green solution left after the removal of the crystals of **4** revealed, besides a small amount of **4** ($g$ = 1.967), a second species with a more intense set of signals with $g$ = 1.999. The latter species is tentatively assigned to a vanadium(II) species with two coordinated THF molecules, similar to the vanadium(II) complex stabilized with TMEDA and successfully characterised by Choukroun and co-workers.[17]

**4** crystallises in the monoclinic system, space group $P2_1/c$, with one molecule in the asymmetric unit. An ORTEP view of the molecular structure is depicted in Fig. 4 and selected structural parameters are listed in Table 1. The coordination geometry is distorted octahedral as in **3**, with atoms Cl1 and N1 in the axial positions and atoms O1, O2, N2 and Cl2 in the equatorial plane. The *trans* arrangement of the phenolate groups, with an angle of 160° between the rings, constrains the chloride groups to be mutually *cis*. The V–Cl bond distances agree well with those found in an analogous complex having methyl instead of *tert*-butyl substituents on the phenolate rings already mentioned[30] and are only slightly shorter than those observed in the few examples of vanadium(IV) dichloride complexes containing N/O donors reported (2.33 Å < $V^{IV}$–Cl < 2.37 Å).[31] The V–N bond lengths are comparable and V–O bond distances are shorter than in diamine bis(phenolate) vanadium(IV) complexes.[30,32]

### Reactions with oxygen – $O_2$

Complexes **1** and **2** are extremely sensitive to moisture and oxygen. In THF solutions both compounds react with oxygen from dried air to give blue solutions containing vanadium(V) oxido complexes [VO(L)Cl] (L = L1, **5** and L2, **6**) as shown in Scheme 1. Although **5** has been obtained in 75% yield,[25] the formation of the new complex **6** occurs in lower yield with the concurrent appearance of a minor vanadium containing species and ligand degradation. Indeed, the $^1H$ and $^{13}C$ NMR spectra of the blue solid obtained after THF evaporation do not only reveal a complex mixture containing [VO(L2)Cl] (**6**) but also additional aromatic and *tert*-butyl resonances arising from partial decomposition of the ancillary ligand. The $^{51}V$ NMR spectrum in $C_6D_6$ displays a major resonance at $\delta$ = −207.3 ppm and a less intense peak at $\delta$ = −354.7 ppm. The former signal is assigned to **6**, by comparison with the value

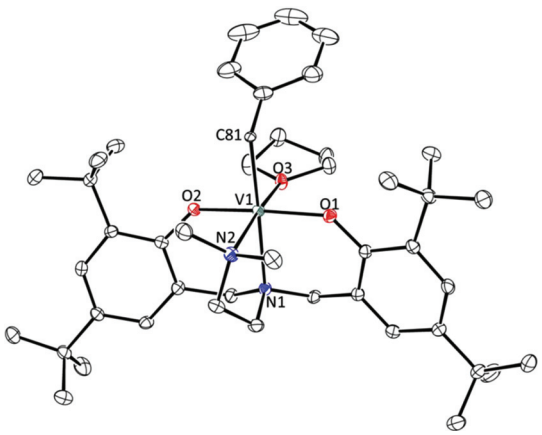


**Fig. 3** ORTEP-3 diagram of **3**, using 40% probability level ellipsoids. Hydrogen atoms and two disordered carbon atoms in the THF fragment are omitted for clarity.

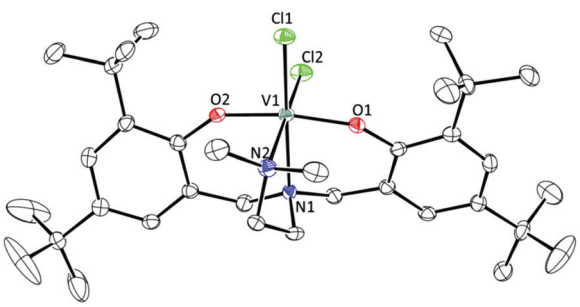


**Fig. 4** ORTEP-3 diagram of **4**, using 40% probability level ellipsoids. Hydrogen atoms are omitted for clarity.

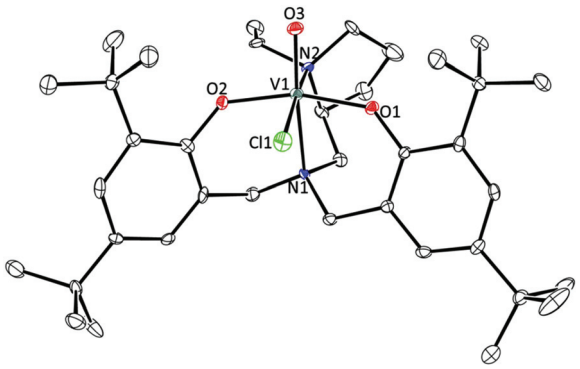


Fig. 5 ORTEP-3 diagram of [VO(L2)Cl] (**6**), using 40% probability level ellipsoids. Hydrogen atoms are omitted for clarity.

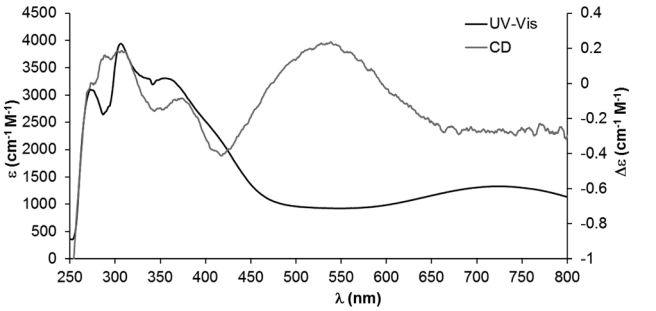


Fig. 6 Isotropic electronic absorption (UV-Vis) and circular dichroism (CD) spectra for complex **6** in chloroform. The UV-Vis and CD spectra were recorded using $6.16 \times 10^{-4}$ M and $1.54 \times 10^{-3}$ M solutions, with 10 and 1 mm optical path cells, respectively.

observed for the vanadium(v) resonance in **5**, but the minor signal could not be identified. The IR spectrum of the blue powder shows a strong band at 998 $cm^{-1}$, characteristic of the V=O stretching mode. Crystals of **6** suitable for single crystal X-ray diffraction were obtained from a solution of the mixture in pentane.

An ORTEP view of **6** is depicted in Fig. 5 and selected structural parameters are listed in Table 1. The compound crystallises in the orthorhombic system, space group *P*222, with one molecule in the asymmetric unit. Atoms O1, O2 and N2 of L2 and the chloride ligand (Cl1) define the equatorial plane, while the oxido ligand (O3) and the tripodal nitrogen N1 occupy the axial positions of the distorted octahedral environment of V(v), with the oxido ligand *trans* to the tripodal nitrogen atom as observed in **5**.[25] Complexes with the oxido ligand *trans* to the tripodal N atom will be called the axial isomers (**5** and **6**), by comparison with species such as **8** where the former ligand is *cis* to the tripodal N atom yielding the equatorial isomer. The ethylpyrrolidine moiety remains coordinated to the metal, in the same $\delta$ conformation as in **2**. The dihedral angle between the *trans* phenolate rings is 125.1(1)° with an arrangement as in **5**,[25] the V=O, V–N, V–Cl and V–$O_{phenolate}$ bond distances being in the expected ranges[17,28,33] and agreeing well with those in **5**.

Fig. 6 shows the isotropic electronic absorption and Circular Dichroism (CD) spectra of solutions of complex **6** in chloroform and Table 2 summarizes the values $\lambda_{max}$ and the corresponding molar absorptivity ($\varepsilon$) of absorption bands, and $\Delta\varepsilon$ from the CD spectra. The absorption spectrum of **6** shows a much less intense absorption band for $\lambda > 500$ nm than **5** and the related chiral complex [$VO(L^{Me})Cl$] ($L^{Me}$ = $Me_2NCH_2CH(CH_3)N(CH_2$-2-*O*-3,5-$C_6H_2{}^tBu_2)_2$),[25] reflecting their structural differences. Considering that **6** is a $d^0$ $V^VO$ species, the strong and broad absorption centred at *ca.* 725 nm is assigned to LMCT bands from the phenolate oxygens to d metal orbitals, giving rise to the intense blue colour. Similar intense CT transitions have been observed for complexes **5** and [$VO(L^{Me})Cl$] and for a few other mono-oxidovanadium(v) phenolate complexes.[34] The CD spectrum of **6** confirms that this complex is optically active. Similarly to what was observed for the previously reported chiral tripodal complex [$VO(L^{Me})Cl$], a transmission of chirality to the intraligand CT transitions is present and CD bands are observed in the 250–300 nm range, although the chiral carbon centre is a few bonds away from the phenolate rings.

Table 2 Isotropic absorption data (UV-Vis) and circular dichroism (CD) data for complex **6**

| UV-Vis | | CD | |
|---|---|---|---|
| $\lambda_{max}$/nm | $\varepsilon$/$M^{-1}$ $cm^{-1}$ | $\lambda_{max}$/nm | $\Delta\varepsilon$/$M^{-1}$ $cm^{-1}$ |
| 306 | 3938 | 311 | +0.18 |
| 355 | 3311 | 352 | −0.15 |
| 430 | 1837 | 426 | −0.38 |
| | | 539 | +0.24 |
| 725 | 1329 | 770 | +0.47 |

The oxidation of [V(L2)Cl] (**2**) to [VO(L2)Cl] (**6**) is accompanied by an increase in the metal coordination number (Scheme 1) and rearrangement, as it involves the shift of the chloride ligand from *trans* to *cis* to the tripodal nitrogen. The oxygen atom of the new V=O fragment is placed *trans* to the tripodal nitrogen, which affords the most stable oxidovanadium isomer supported by diamine bis(phenolate) ligands as shown by DFT calculations performed for [VO(L1)Cl] (**5**).[25]

In order to confirm that the $O_2$ present in air (and not moisture) is responsible for the oxidation of vanadium(III) in complex **2**, deaerated water was added to a red solution of **2** in toluene and the mixture was vigorously stirred. No colour change was observed even after 12 h of stirring. However, when a portion of this mixture was exposed to air, the colour immediately changed to blue. This observation clearly shows that **2** is oxidised by $O_2$, probably as a result of coupling between two diradical species. Although reactions of V(III) complexes with oxygen have been reported, only very few vanadium(III) compounds could be oxidized by $O_2$ to their oxidovanadium(v) complexes.[16,19,35,36] Attempts to understand the mechanism of the oxidation of V(III) to V(v) by oxygen led us to perform reactions of crystalline samples of [V(L2)Cl] with dried air or $O_2$ either in the solid state or in solution. The

main conclusion from these attempts is that pure **6** could only be obtained when crystalline samples of **2** were exposed to very slow diffusion of air. When the contact of oxygen with the compound is not controlled by diffusion, ligand deterioration accompanies the formation of **6**. The clue for the understanding of this result was obtained accidentally from the solid-state reaction of a mono-crystal of **2**, covered with perfluoroether oil, with $O_2$ in air to give [V($\eta^2$-$O_2$)L2Cl] (**7**, Scheme 1).

Complex **7** is only the second non-oxido vanadium peroxido derivative reported to date.[35] Its formation took place after a few hours at room temperature as attested by the colour change of the crystal from red to blue. The X-ray diffraction data of **7** are of low quality, but the structure was unequivocally determined and revealed the formation of a new $\eta^2$-peroxido ligand that results from the diradical coupling of oxygen with the $d^2$-vanadium centre. An ORTEP view of the molecular structure is depicted in Fig. 7 and selected structural parameters are listed in Table 1.

**7** crystallises in the monoclinic system, space group $P2_1$, with one molecule in the asymmetric unit. The metal seven-coordination geometry is best described as distorted capped octahedral with the equatorial plane defined by atoms O1, O2 and N2 of the diaminebisphenolate ligand and atom O3 of the peroxido ligand. The axial positions are occupied by the tripodal nitrogen N1 and the chloride ligand (Cl1), while atom O4 of the peroxido ligand caps the O1–O3–Cl1 face of the octahedron. To facilitate comparison with others, the structure of **7** can also be described as distorted octahedral, considering the middle point of the O3–O4 bond (m) as the sixth ligand, after the aminophenolate and the chloride. Indeed, the m-V–N2 angle is close to 177°.

The chloride ligand remains *trans* to the tripodal nitrogen, as in the trigonal bipyramidal **2**, indicating that the oxidative addition of molecular oxygen to **2** occurred with a minimal distortion of the latter complex structure and an equatorial isomer has formed. The V–$O_{phenolate}$ and V–Cl bond distances are shorter than in the vanadium(III) complex **2**, although the V–N bond distances are significantly longer than in **2**. The lengthening of the V1–N2 distance, in particular, may be associated with the *trans* influence of the peroxido group.

The distances between vanadium and the peroxido oxygen atoms in oxidoperoxidovanadium(V) complexes with O- and N-based ligands are usually very similar, their difference ranging from 0.01 and 0.023 Å in several reported structures.[37] In **7**, however, this difference is 0.07 Å ($d$(V1–O3) = 1.78(2) Å, $d$(V1–O4) = 1.85(1) Å) and the O3–O4 bond length is 1.39(2) Å, revealing a significant elongation of the O–O distance upon coordination ($d_{O-O}$ in $O_2$ is 0.121 Å). The metric parameters determined for **7** are close to those reported for [($\eta^2$-$O_2$)V(N-[$^t$Bu]Ar)$_3$],[35] which is the unique non-oxido complex of vanadium displaying an $\eta^2$-$O_2$ ligand and formally seven-coordinate, although the O–O bond length in the latter complex is slightly longer (1.416(5) Å) than in **7**.

### Reactions with $O_2$ – mechanism

Density functional theory calculations (GAUSSIAN 03/PBE1PBE, see Computational details) were performed in order to understand whether the peroxido complex **7** might be an intermediate in the formation of **6** from the reaction of **2** with $O_2$ (Scheme 2). Simplified models, with methyl instead of *tert*-butyl aromatic substituents, were used for the calculations. The optimised geometries of the models (represented with *) reproduce the experimental available ones (see the ESI†).

Two intermediates may be envisaged for the reaction of **2** with $O_2$, a side-bound peroxido complex (**7***) or an end-bound peroxido complex (**A**) being not detected. Both intermediates **7*** or **A** may react further with a second equivalent of vanadium(III) complex **2*** to give the dimeric intermediate **B**, which converts to the oxido complex **6*** by cleavage of the O–O bond (Scheme 2). An additional difficulty arises from the different ligand arrangements around vanadium in structurally characterized **7** and **6** (**7*** and **6*** in the models), as **7** is an equatorial isomer and **6** is an axial one (see definitions above).

The overall reaction of 2 moles of vanadium(III) complex **2*** and one mole of $O_2$ to yield two moles of **6*** is a favourable thermodynamic process ($\Delta G_{298}$ = −38.3 kcal mol$^{-1}$). On the other hand, the oxidative addition of $O_2$ to form any of the side-bound $\eta^2$-$O_2$ (**7***) or end-bond $\eta^1$-$O_2$ (**A**) peroxido inter-

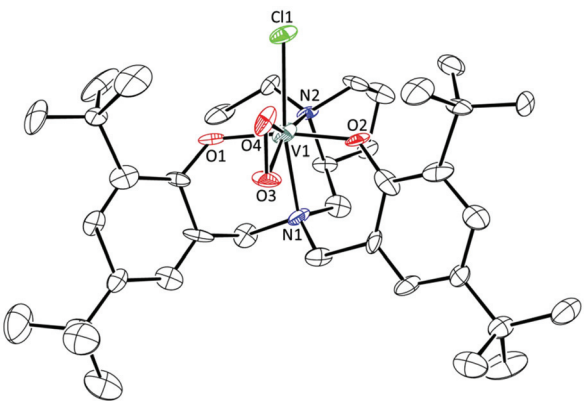


**Fig. 7** ORTEP-3 diagram of [V($\eta^2$-$O_2$)L$^3$Cl] (**7**), using 30% probability level ellipsoids. Hydrogen atoms are omitted for clarity.

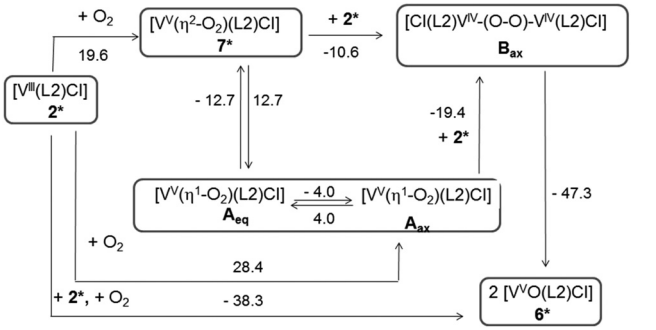


**Scheme 2** Gibbs energy for alternative pathways leading to the formation of **6** from **2** and $O_2$ ($\Delta G_{298}$ in kcal mol$^{-1}$), modelled with methyl instead of *tert*-butyl groups (**7***, **6*** and **2***).

mediates in the first step is an endergonic process (9 kcal $mol^{-1}$). These species are high energy intermediates. $\eta^2$-$O_2$ (**7***) is the more stable dimer and corresponds to the dimer experimentally obtained in the solid state reaction described above. Besides being the thermodynamic favoured species, formation of **7*** should require less distortion of the initial complex **2*** (kinetic isomer). The side-bound peroxido intermediate **7*** is thus the most likely intermediate, although the difference between the $\Delta G$ values of **7*** and **A** is small.

On the other hand, in order to form the dimeric intermediate **B**, one of the peroxide oxygen atoms must coordinate to one incoming V(III) complex **2***. This may happen immediately from the peroxido end-bound intermediate **A**, but not from the peroxido side-bound intermediate **7***, which must rearrange. Therefore, intermediate **7*** should isomerise to **A**. The $\eta^2$- to $\eta^1$-$O_2$ shift will lead to the equatorial isomer ($\mathbf{A_{eq}}$), which needs to convert into the more stable $\mathbf{A_{ax}}$ isomer in order to obtain the right arrangement of the final product **6***. The small energy differences between the intermediates **7***, $\mathbf{A_{eq}}$ and $\mathbf{A_{ax}}$ suggest that there may be an equilibrium between them. Therefore, the second reaction step should be the isomerisation from **7*** to $\mathbf{A_{eq}}$ followed by isomerisation from $\mathbf{A_{eq}}$ to $\mathbf{A_{ax}}$. In the third step, $\eta^1$-$O_2$ ($\mathbf{A_{ax}}$) reacts with a second molecule of **2*** to yield the bridged peroxide dimer **B** (axial isomer). Cleavage of the O–O bond in dimer **B** gives the oxido vanadium(v) species **6*** (axial isomer).

A similar reaction between $[V(N\{tBu\}Ar)_3]$ and $O_2$ led to $[V(\eta^1\text{-}O_2)(N\{tBu\}Ar)_3]$, which isomerized to the more stable (4.2 kcal $mol^{-1}$) $\eta^2$-$O_2$ and ended in an oxido vanadium(v) complex.[35] $[V(\eta^2\text{-}O_2)(N\{tBu\}Ar)_3]$ was synthesized by a different route (solution) from the one described above and was structurally characterized as the first example of a vanadium(v) complex with one side-on $\eta^2$-$O_2$ peroxide in the absence of any V=O bonds. Complex **7** described above is the second example and resulted from a solid state reaction. Also, it is formed directly from complex **2** and $O_2$. The energy difference between the $\eta^1$ and $\eta^2$-$O_2$ is higher in our system (8.7 kcal $mol^{-1}$) and this is one reason that may have prevented its detection. These differences probably arise from the different coordination environment of the two complexes, five in $[V(\eta^2\text{-}O_2)(N\{tBu\}Ar)_3]$ and seven in **7**. The formation of the final oxido vanadium(v) complex probably follows the same route, *via* a dimeric V(v) complex with a bridging peroxide, in both systems.

We therefore propose that the mechanism to obtain the oxidovanadium(v) complex **6** (Scheme 2) involves the $\eta^2$-$O_2$ complex (**7**), its isomerization to an $\eta^1$-$O_2$ complex, reaction with another molecule of the V(III) complex **2** to form the dimer **B** and its cleavage.

### Reactions with TEMPO

[VO(L1)Cl] (**5**) and [VO(L2)Cl] (**6**) were also obtained through the reactions of vanadium(III) complexes **1** and **2** with one equivalent of the nitroxyl radical TEMPO in toluene. The $^1$H NMR of the blue solids obtained after evaporation of the solvent revealed the presence of the oxidovanadium(v) complexes **5** and **6** and TEMPO–$CH_2$Ph in 1 : 0.5 and 1 : 1.3 ratios, respectively.[38] Complexes **5** and **6** were obtained in about 50% yield, which suggests that only one-half of the TEMPO radicals reacts with the vanadium(III) complexes. The other half yields TEMPO–$CH_2$Ph in 23% and 66%, respectively, through reaction with the toluene solvent. Surprisingly, reactions of **1** and **2** with 2 equivalents of TEMPO only led to a slight increase in the yields of **5** and **6**.

The mechanism of these reactions most likely involves the coordination of TEMPO to the vanadium followed by oxygen abstraction leading to the oxidovanadium complexes **5** and **6** and a piperidyl radical (Scheme 3). This radical may react with toluene to give 2,2,6,6-tetramethylpiperidine and a benzyl radical that leads to the formation of TEMPO–$CH_2$Ph upon radical coupling with TEMPO. DFT calculations (GAUSSIAN 09/UPBE1PBE, see Computational details) showed that the overall reaction of 2 moles of TEMPO with one mole of **2** and one mole of toluene to give one mole of TEMPO–$CH_2$Ph, one mole of **6** and one mole of piperidine is a favourable process from the thermodynamic point of view ($\Delta G_{298}$ = −2.8 kcal $mol^{-1}$).

### Alternative synthetic routes to V(v)=O complexes

Since the oxidation of compound **2** in air revealed to be a low yield method for the preparation of the corresponding oxidovanadium(v) complex **6**, an alternative synthetic procedure for the preparation of **6** was searched. The reaction of $VOCl_3$ with the sodium salt $Na_2L2$, for instance, gave a dark blue solution upon contact of the reagents but it turned dark green after overnight reaction. A dark greenish solid was obtained after workup. Spectroscopic data were inconclusive and no crystals could be obtained.

A fruitful procedure for the synthesis of an oxidovanadium(v) complex supported by ligand L2 was finally found using $[VO(O^iPr)_3]$ as a starting material. The reaction of $[VO(O^iPr)_3]$ with $H_2L2$ gave $[VO(L2)(O^iPr)]$ (**8**) as a dark brownish solid with 60% yield. The $^1$H NMR spectrum reveals a rigid asymmetric complex presenting distinct resonances for all protons. A second set of peaks of much lower intensity, at slightly different chemical shifts and with the same multiplicity, is also observed, which is indicative of the presence of a minor isomer in a ratio of 1 : 10. Four isomers of complex **8** are poss-

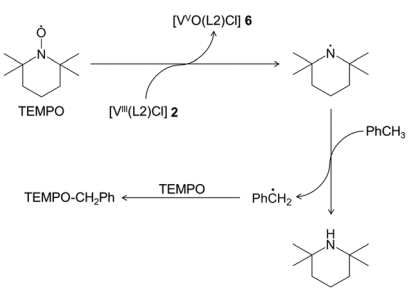


**Scheme 3** Possible reactions leading to the formation of TEMPO–$CH_2$Ph.

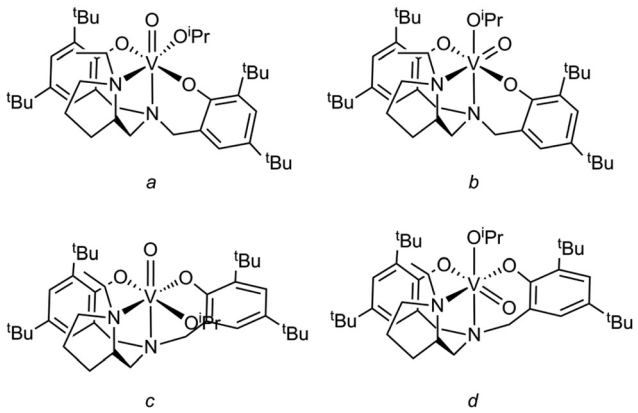


Fig. 8 Four possible isomers of **8**.

ible (*a–d* in Fig. 8). However, previous studies have shown that *trans*-phenolate configurations (*a* and *b*) are usually more stable than *cis*-phenolate isomers (*c* and *d*).[22,25] Additionally, brownish crystals of **8** suitable for X-ray diffraction were grown from a toluene/hexane solution and the structure obtained corresponds to isomer *b* displaying *trans* phenolates and the O$^i$Pr ligand *trans* to the tripodal nitrogen. This is the same isomer that was structurally determined for the analogous complex with L1 and that was shown, by DFT calculations, to be the most stable isomer.[25] Thus, the mixture of isomers revealed by NMR is most likely a mixture of isomers *a* and *b* in a 1 : 10 ratio. In the case of L1 a ratio of 1 : 2 of *a* and *b* isomers was obtained while in the case of L2 a higher amount of isomer *b* is formed. This must be related with the higher steric constraint imposed by the bulkier ethylpyrrolidine moiety, leaving less space in the equatorial plane for the coordination of the isopropoxido ligand.

Compound **8** crystallises in the monoclinic system, space group $P2_1$, with four molecules in the asymmetric unit. As shown in Fig. 9, the four molecules **8** (*1–4*) differ mainly in the coordination mode of the diamine side arm. An ORTEP view of one of the molecules, **8**(*1*), is depicted in Fig. 10 and selected structural parameters are listed in Table 1. Compound **8** presents distorted octahedral geometry similarly to **6**. The structure obtained corresponds to isomer 8*b* with the oxido ligand *cis* to the tripodal nitrogen, as observed for [VO(L1)(O$^i$Pr)], synthesized and characterized in previous studies.[25] The V=O, V–O$_{phenolate}$ and V–O$^i$Pr bond distances are in the ranges found for isopropoxido oxidovanadium(v) complexes.[17,28,33,39] The phenolate moieties adopt a *trans* configuration bending towards the oxido ligand and define dihedral angles of 109.71(1)° to 121.72(1)° between the aromatic planes.

### V(v)=O complexes in catalytic sulfoxidation

The oxidovanadium(v) complex **5** and the chiral analogue [VO(L$^{Me}$)Cl] had been found to be very selective towards thioanisole sulfoxidation in previous studies. However, no enantioselectivity was achieved when the chiral complex was used as the catalyst precursor.[25]

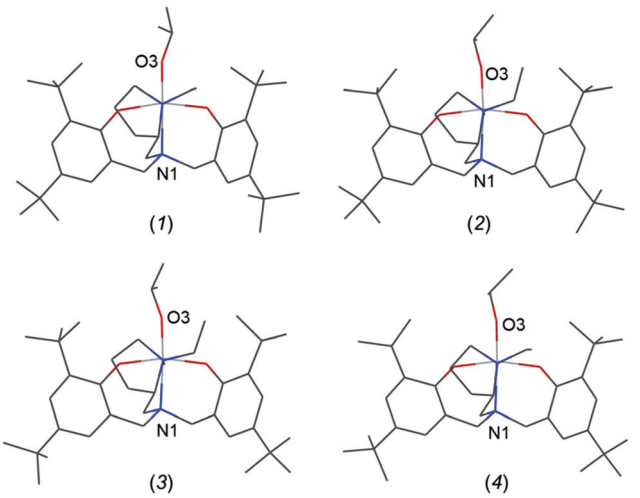


Fig. 9 Wireframe diagrams of the four molecules of **8** present in the asymmetric unit.

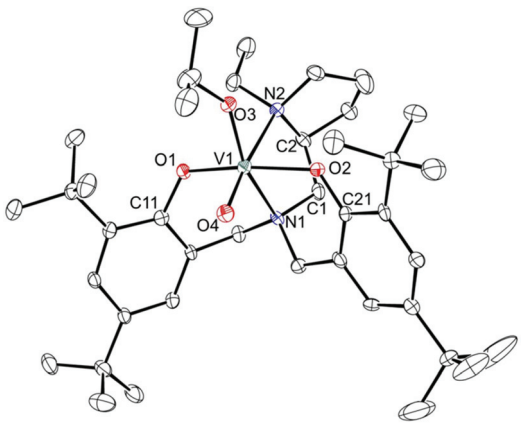


Fig. 10 ORTEP-3 diagram of **8**(*1*), using 40% probability level ellipsoids. Hydrogen atoms are omitted for clarity.

Complexes **6** and **8**, which contain a bulkier chiral moiety in the ligand framework, were tested in the sulfoxidation of thioanisole. Under the reaction conditions (1–2 mol% catalyst, 10 °C, $H_2O_2$ as an oxidant and 1,2-dichloroethane as a solvent), near-complete conversions were obtained but no enantioselectivity was achieved (see Table S1, ESI†). This result is in line with other attempts reported in the literature and points out that the use of $H_2O_2$ as a terminal oxidant in enantioselective sulfoxidation requires either the addition of an excess of chiral ligands to metal precursors or the use of surfactants.[40] The huge potential of chiral sulfoxides would justify the development of well-defined catalysts but unfortunately, with the exception of the Fe salan complexes reported by Katsuki,[41] these still remain elusive species.

# Concluding remarks

Vanadium(III) complexes supported by a chiral tripodal diamine bisphenolate ligand that displays a ethylpyrrolidine group (**1**) are described and compared with related non-chiral complexes of the same type, previously described, having a dimethylamine donor group (**2**). The bulkiness of the ethylpyrrolidine group is responsible for the differences, namely the vanadium coordination geometry, trigonal bipyramidal in **2** and octahedral in **1** with one additional THF ligand. This results in an important difference in the reactivity of the two complexes with oxygen. The vanadium in complex **2** is able to coordinate one molecule of oxygen that binds in an $\eta^2$-$O_2$ mode in the solid without a significant disruption of the ancillary ligand coordination. Complex **7** is the second example of a structurally characterized non-oxido peroxidovanadium(V) complex, and the first obtained through a solid state reaction.

DFT calculations showed that **7** is a reactive species that through $\eta^2/\eta^1$ isomerization of the peroxido ligand may react with **2** to give **6**. The process of conversion of **2** in **6** is fairly clean when the reaction of **2** with oxygen is controlled by slow diffusion of $O_2$ into a crystalline sample of **2** but it results in partial ligand decomposition in other experimental conditions. This reaction is thus an example of the control that may be exerted by a specific environment on the outcome of a chemical reaction, as it happens in many processes involving lock and key fitting. Indeed, the formation of **7** from the oxidative addition of molecular oxygen to **2** involving a minimal disturbance of the complex structure, the pentacoordinated vanadium coordination sphere with oxygen and nitrogen atoms, and the trigonal bipyramidal geometry of **2** are features that make this complex a model of vanadium haloperoxidases.[42]

The reaction of **2** with the radical TEMPO revealed that after oxygen transfer to vanadium forming **5**, the piperidyl radical captures a radical from the solvent generating a benzyl radical that competes with vanadium to react with TEMPO. An aspect that may be critical in this reaction is the bulkiness of both V(III) complex and TEMPO.

The high yield synthesis of complex **8**, an analogue of **6** with a terminal V=O bond, was made possible when Cl was replaced by $O^iPr$ in the $VOX_3$ reagent. Interestingly, in the major species in solution, the oxido ligand occupies the equatorial, rather than the axial position, contrary to **6**. Although extremely active and selective in sulfoxidation catalysis, the complexes described are not enantioselective.

# Experimental

### General considerations

All preparations and subsequent manipulations of air/moisture sensitive compounds were performed under a nitrogen atmosphere using standard Schlenk line and glovebox techniques. THF, toluene, pentane, *n*-hexane and $Et_2O$ were dried by standard methods (sodium/benzophenone for THF, toluene and $Et_2O$; calcium hydride for *n*-hexane and pentane) and distilled prior to use. $C_6D_6$ was dried over Na and distilled under reduced pressure. $CDCl_3$ was dried with 4 Å and degassed by the freeze–pump–thaw method. Unless stated otherwise, all reagents were purchased from commercial suppliers (*e.g.* Aldrich, Acrös, Fluka) and used as received. Commercial NaH (60% dispersion in mineral oil) was washed with *n*-hexane and dried under vacuum. $H_2L1$ [26] and $VCl_3(THF)_3$ [43] were synthesized following literature procedures; $H_2L2$ [26] and [V(L1)Cl(THF)][20] were prepared as previously published. 1D ($^1H$, $^{13}C\{^1H\}$, $^{51}V$) and 2D NMR spectra were recorded with Bruker Avance II+ 300 and 400 MHz (UltraShield Magnet) spectrometers at ambient temperature. $^1H$ and $^{13}C$ chemical shifts ($\delta$) are expressed in ppm relative to $Me_4Si$ and $^{51}V$ was referenced to external neat $VOCl_3$. NMR samples of air/moisture sensitive compounds were prepared in a glovebox under an inert atmosphere using NMR tubes equipped with J-Young stopcocks. The magnetic susceptibility was determined for powdered samples of the compounds using a SHERWOOD SCIENTIFIC Magnetic Susceptibility Balance based on the Evans method. Diamagnetic corrections for the diamino-bisphenolate ligand were applied. Elemental analyses were carried out using an EA110 CE Instruments automatic analyser. The electron paramagnetic resonance (EPR) spectra were measured with a Bruker ESP 300E X-band spectrometer, in frozen samples at 77 K.

### Synthesis of [V(L2)Cl], 2

A solution of $H_2L2$ (0.847 g, 1.5 mmol) in THF was slowly added to NaH (0.079 g, 3.3 mmol) and the mixture was stirred for 1.5 h at room temperature. The colourless solution obtained was filtered through a Celite layer and added to a suspension of $VCl_3(THF)_3$ (0.542 g, 1.5 mmol) in THF at −30 °C. The temperature was allowed to rise slowly and the solution was further stirred for 4 h at room temperature. The red solution obtained was filtered and evaporated to dryness leading to a red microcrystalline powder. Yield: 0.900 g, 92%. Red crystals of **2** suitable for X-ray diffraction were obtained from $Et_2O$ at −20 °C. $\mu_{eff}$ (18 °C) = 2.36$\mu_B$. EA calculated for $C_{37}H_{58}ClN_2O_2V$: C, 68.45; H, 9.00; N, 4.31. Found: C, 64.19; H, 7.01; N, 5.65 (attempts to obtain good elemental analysis failed due to the instability of the compound).

### Synthesis of [V(L1)($CH_2Ph$)(THF)], 3

A solution of 1.64 M $PhCH_2MgCl$ in $Et_2O$ (0.35 mL, 0.58 mmol) was added to a solution of **1** (0.389 g, 0.58 mmol) in toluene at −80 °C. The temperature was allowed to rise slowly to room temperature and the solution was further stirred for 7 h. The green solution obtained was evaporated to dryness, and the residue was extracted with $Et_2O$ and the solution was filtered. Evaporation of the $Et_2O$ solution to dryness led to a green crystalline solid. Yield: 0.320 g, 82%. Green crystals of **3** suitable for X-ray diffraction were obtained from $Et_2O$ at −20 °C. $\mu_{eff}$ (25 °C) = 2.57$\mu_B$. EA calculated for $C_{45}H_{69}N_2O_3V$: C, 73.34; H, 9.44; N, 3.80. Found: C, 65.43; H, 9.83; N, 3.92 (attempts to obtain good elemental analysis failed due to the instability of the compound).

### Synthesis of [VO(L2)Cl], 6

A red solution of **2** in THF was exposed to air, through a $CaCl_2$ drying tube, for 18 h. The blue solution obtained was filtered and evaporated to dryness leading to a blue powder. The NMR experiments revealed a mixture of **6** with fragments of the ligand. Crystals of **6** suitable for X-ray diffraction were obtained from a pentane solution of the mixture at +4 °C. Pure **6** was obtained when a sample of crystals of **2** was exposed to air in a controlled way (very slow diffusion of air into the Schlenk tube containing crystals of **2**). $^1$H NMR (300 MHz, $C_6D_6$, ppm): $\delta$ 7.63 (d, 1H, $^4J_{HH}$ = 2.2 Hz, C*H*–Ar), 7.48 (d, 1H, $^4J_{HH}$ = 2.2 Hz, C*H*–Ar), 7.13 (overlapped by a solvent peak, C*H*–Ar), 6.81 (d, 1H, $^4J_{HH}$ = 1.9 Hz, C*H*–Ar), 5.43 (d, 1H, $^2J_{HH}$ = 14.7 Hz, NC$H_2$Ar), 4.36 (m, 1H, C$H_2$), 3.67 (d, 1H, $^2J_{HH}$ = 13.3 Hz, NC$H_2$Ar), 3.55 (m, 1H, C$H_2$), 3.02 (m, 1H, C$H_2$), 2.97 (d, 1H, $^2J_{HH}$ = 14.9 Hz, NC$H_2$Ar), 2.71 (m, 2H, C$H_2$ + C*H*), 2.55 (m, 2H, NC$H_2$Ar + C$H_2$), 1.87 (s, 9H, C(C$H_3$)$_3$), 1.77 (s, 9H, C(C$H_3$)$_3$), 1.40 (s, 9H, C(C$H_3$)$_3$), 1.31 (m, 1H, C$H_2$), 1.29 (m, 3H, $CH_2CH_3$), 1.26 (s, 9H, C(C$H_3$)$_3$), 1.23 (m, 2H, C$H_2$), 1.04 (m, 1H, C$H_2$), 0.33 (m, 1H, C$H_2$). $^{13}$C–{$^1$H} NMR (75 MHz, $C_6D_6$, ppm): $\delta$ 168.5, 165.4, 146.5, 145.0, 136.2, 133.8, 126.9 and 126.3 ($C_{ipso}$–Ar), 124.4, 124.3, 124.1 and 122.3 (*C*H–Ar), 64.2 (*C*H), 62.2 (N*C*H$_2$Ar), 60.1 (*C*H$_2$), 59.5 (N*C*H$_2$Ar), 58.4 and 56.7 (*C*H$_2$), 35.9, 35.8, 34.8 and 34.7 (*C*(CH$_3$)$_3$), 31.9, 31.7, 31.3 and 31.1 (C(*C*H$_3$)$_3$), 27.3 and 24.3 (*C*H$_2$), 11.4 ($CH_2$*C*H$_3$). $^{51}$V NMR (79 MHz, $C_6D_6$, ppm): $\delta$ −207.3. FT-IR (KBr, cm$^{-1}$): $\nu$(V=O) 998. EA calculated for $C_{37}H_{58}ClN_2O_3V{\cdot}1.5(H_2O)$: C, 64.20; H, 8.88; N, 4.05. Found: C, 63.95; H, 8.72; N, 3.94.

### Reaction of 1 with TEMPO

A solution of 2,2,6,6-tetramethylpiperidine-1-oxyl (TEMPO) (0.365 g, 0.55 mmol) in toluene was added to a solution of **1** (0.086 g, 0.55 mmol) in the same solvent at −50 °C. The temperature was allowed to rise slowly to room temperature and the solution was further stirred overnight. The blue solution obtained was filtered and evaporated to dryness giving a blue solid. The NMR data revealed a mixture of **5** and TEMPO–$CH_2$Ph in a 1 : 0.5 ratio. Yield of **5**: 50%. Detailed NMR data for TEMPO–$CH_2$Ph are available in the ESI.†

### Reaction of 2 with TEMPO

A solution of 2,2,6,6-tetramethylpiperidine-1-oxyl (TEMPO) (0.400 g, 0.62 mmol) in toluene was added to a solution of **2** (0.096 g, 0.62 mmol) in the same solvent at −50 °C. The temperature was allowed to rise slowly to room temperature and the solution was further stirred overnight. The blue solution obtained was filtered and evaporated to dryness giving a blue solid. The NMR experiments revealed a mixture of **6** with TEMPO–$CH_2$Ph in a 1 : 3 ratio. Yield of **6**: 48%.

### Synthesis of [VO(L2)(O$^i$Pr)], 8

$VO(OiPr)_3$ (0.24 ml, 1.0 mmol) was slowly added to a solution of $H_2$L2 (0.57 g, 1.0 mmol) in 5 ml THF. The mixture was stirred overnight, and then the solvent was evaporated under reduced pressure. The resulting dark brownish product was extracted in diethyl ether and again evaporated and dried under reduced pressure to give a dark purple solid. Yield: 0.413 g, 60%. Dark brown crystals of **8** suitable for X-ray diffraction were obtained from a toluene/hexane mixture at −4 °C. $^1$H NMR (400 MHz, $CD_2Cl_2$, ppm): $\delta$ 7.38 (d, $^4J_{HH}$ = 2.4 Hz, 1H, C*H*–Ar), 7.20 (d, $^4J_{HH}$ = 2.5 Hz, 1H, C*H*–Ar), 7.16 (d, $^4J_{HH}$ = 2.4 Hz, 1H, C*H*–Ar), 6.90 (d, $^4J_{HH}$ = 2.3, 1H, C*H*–Ar), 5.55 (sept, 1H, OC*H*(CH$_3$)$_2$), 4.91 (d, $^2J_{HH}$ = 15.3 Hz, 1H, ArC$H_2$N), 4.26 (d, 1H, $^2J_{HH}$ = 12.3 Hz, ArC$H_2$N), 3.93 (m, 1H, C$H_2$), 3.63 (d, $^2J_{HH}$ = 15.3 Hz, 1H, ArC$H_2$N), 3.42 (m, 1H, C*H*), 3.16 (d, 1H, $^2J_{HH}$ = 12.2 Hz, ArC$H_2$N), 3.03 (m, 2H, C$H_2$), 3.00 (m, 1H, C$H_2$), 2.79 (m, 1H, C$H_2$), 2.23 (m, 1H, C$H_2$), 1.87 (m, 1H, C$H_2$), 1.81 (m, 2H, C$H_2$), 1.55 (d, $^2J_{HH}$ = 6.1, 3H, OCH(C$H_3$)$_2$), 1.49 (s, 9H, C(C$H_3$)$_3$), 1.47 (d, 3H, OCH(C$H_3$)$_2$, partially overlapped by a *tert*-butyl signal) 1.45 (s, 9H, C(C$H_3$)$_3$), 1.35 (s, 9H, C(C$H_3$)$_3$), 1.26 (s, 9H, C(C$H_3$)$_3$), 1.14 (m, 3H, C$H_3$). $^{13}$C–{$^1$H} NMR (101 MHz, $CD_2Cl_2$, ppm): $\delta$ 166.3, 162.6, 141.2, 141.1, 135.9, 134.6 ($C_{ipso}$–Ar), 124.4 (*C*H–Ar), 124.3 ($C_{ipso}$–Ar), 124.3 and 123.6 (*C*H–Ar), 122.7 ($C_{ipso}$–Ar), 122.0 (*C*H–Ar), 83.8 (O*C*H(CH$_3$)$_2$), 63.9 (N*C*H$_2$Ar), 63.4 (*C*H$_2$), 62.2 (*C*H), 61.1 (N*C*H$_2$Ar), 54.3 and 52.8 (*C*H$_2$), 35.7, 35.6, 34.7 and 34.6 (*C*(CH$_3$)$_3$), 32.1, 31.9, 31.1 and 30.9 (C(*C*H$_3$)$_3$), 29.4 and 25.7 (*C*H$_2$), 25.4 and 24.7 (OCH(*C*H$_3$)$_2$), 11.2 (*C*H$_3$). $^{51}$V NMR (79 MHz, $C_6D_6$, ppm): $\delta$ −402.2 (major isomer), −499.6 (minor isomer). FT-IR (KBr, cm$^{-1}$): $\nu$(V=O) 984. EA calculated for $C_{40}H_{65}N_2O_4V{\cdot}0.5(C_7H_8)$: C, 64.83; H, 8.63; N, 3.48. Found: C, 64.59; H, 8.78; N, 3.64.

### Sulfoxidation of thioanisole

The catalytic experiments were carried out at atmospheric pressure, at a constant temperature, in a glass batch reactor, equipped with a magnetic stirrer, thermometer and condenser. In a typical run, the solid catalyst (1 or 2 mol%) and thioanisole (1 mmol) were dissolved in 1,2-dichloroethane (4 mL). Then the oxidant (1.1 mmol), hydrogen peroxide (30 wt% aqueous solution) or TBHP (5.5 M in decane), was added to the mixture under stirring. Control experiments were carried out in the absence of a catalyst. Samples of the reaction mixture were withdrawn and analyzed on a Jasco HPLC system equipped with a Daicel Chiralpak IA column. The eluent used was hexane : ethyl acetate (60 : 40) with a flow rate of 1 mL min$^{-1}$. The calibration curves for each reagent and product, namely sulfide, sulfoxide and sulfone, were determined using similar HPLC procedures and these calibrations were used for the quantitative analyses. Diphenylsulfone was used as an internal standard.[9]

### Crystallographic data

Crystals suitable for single-crystal X-ray analysis were grown as described in the synthetic procedures. Selected crystals were covered with polyfluoroether oil and mounted on a nylon loop (air/moisture sensitive compounds were selected and mounted inside a glovebox). The data were collected using graphite monochromated Mo-K$_\alpha$ radiation ($\lambda$ = 0.71073 Å) on a Bruker AXS-KAPPA APEX II diffractometer equipped with an Oxford Cryosystem open-flow nitrogen cryostat. Cell parameters were

 

Table 3 Selected crystallographic experimental data and structure refinement parameters for **2**, **3**, **4**, **6**, **7** and **8**

| | **2** | **3** | **4** | **6** | **7** | **8** |
|---|---|---|---|---|---|---|
| Empirical formula | $C_{37}H_{58}ClN_2O_2V\cdot(C_4H_{10}O)$ | $C_{45}H_{69}N_2O_3V\cdot(C_4H_{10}O)$ | $C_{34}H_{54}Cl_2N_2O_2V$ | $C_{37}H_{58}ClN_2O_3V$ | $C_{37}H_{58}ClN_2O_4V$ | $C_{40}H_{65}N_2O_4V$ |
| Formula weight | 723.36 | 811.08 | 644.63 | 665.24 | 681.24 | 688.88 |
| Temperature (K) | 150(2) | 150(2) | 150(2) | 150(2) | 150(2) | 293(2) |
| Crystal system | Monoclinic | Monoclinic | Monoclinic | Orthorhombic | Monoclinic | Monoclinic |
| Space group | $P2_1$ | $P2_1/c$ | $P2_1/c$ | $P2_12_12_1$ | $P2_1$ | $P2_1$ |
| $a$ (Å) | 14.3330(8) | 10.4460(4) | 16.783(6) | 9.997(2) | 14.468(11) | 15.5180(11) |
| $b$ (Å) | 8.3560(4) | 22.8520(9) | 15.451(7) | 12.560(3) | 7.746(5) | 23.5210(10) |
| $c$ (Å) | 17.3390(9) | 19.6630(7) | 15.217(7) | 28.755(6) | 17.587(13) | 21.8270(10) |
| $\alpha$ (°) | 90 | 90 | 90 | 90 | 90 | 90 |
| $\beta$ (°) | 100.892(3) | 101.824(2) | 116.088(10) | 90 | 112.27(2) | 100.875(2) |
| $\gamma$ (°) | 90 | 90 | 90 | 90 | 90 | 90 |
| $V$ (Å$^3$) | 2039.22(18) | 4594.2(3) | 3544(3) | 3610.5(13) | 1824(2) | 7823.8(7) |
| $Z$, $\rho_{calc}$ (g cm$^{-3}$) | 2, 1.178 | 4, 1.173 | 4, 1.208 | 4, 1.224 | 2, 1.240 | 8, 1.170 |
| $\mu$ (mm$^{-1}$) | 0.346 | 0.260 | 0.461 | 0.385 | 0.385 | 0.293 |
| Crystal size | 0.40 × 0.08 × 0.04 | 0.40 × 0.20 × 0.05 | 0.30 × 0.20 × 0.10 | 0.08 × 0.08 × 0.02 | 0.30 × 0.18 × 0.04 | 0.18 × 0.18 × 0.04 |
| Crystal colour | Red | Green | Blue | Blue | Blue | Brown |
| Crystal shape | Prism | Plate | Prism | Plate | Prism | Block |
| Refl. collected | 22 024 | 47 432 | 23 383 | 39 525 | 16 581 | 48 637 |
| Unique refl. [$R$(int)] | 10 555 [0.0417] | 8110 [0.0624] | 6714 [0.1028] | 6353 [0.1644] | 5273 [0.1784] | 24 927 [0.0482] |
| $R_1$ [$I > 2\sigma(I)$] | 0.0441 | 0.0485 | 0.0543 | 0.0546 | 0.1199 | 0.0492 |
| w$R_2$ [$I > 2\sigma(I)$] | 0.0949 | 0.1255 | 0.1036 | 0.0848 | 0.2684 | 0.0965 |
| GooF | 1.001 | 1.059 | 0.943 | 0.934 | 0.905 | 0.976 |
| Flack's param. | 0.011(11) | | | −0.02(3) | 0.02(6) | −0.004(10) |

retrieved using Bruker SMART software and refined using Bruker SAINT on all observed reflections. Absorption corrections were applied using SADABS.[44] The structures were solved and refined using direct methods with program SIR2004 [45] using the WINGX-Version 2014.1 [46] SHELXL[47] system of programs.

In compound **3**, two of the carbon atoms of the THF fragment presented disorder and were modelled to 74/26% occupancies. The crystal of **7** had low quality and poor diffracting power; even so, the structure was unequivocally determined.

All non-hydrogen atoms were refined anisotropically and the hydrogen atoms were inserted in idealized positions and allowed to refine riding on the parent carbon atom. The molecular diagrams were drawn with ORTEP-3 for Windows[48] or Mercury 3.8,[49] included in the software package.

For crystallographic experimental data and structure refinement parameters see Table 3. CCDC 1536781–1536786† contain the supplementary crystallographic data for this paper.

### Computational details

DFT[50] calculations for **2***, **6***, **7***, **A** and **B**, **C**, **D**, **E**, **F**, $\mathbf{O_2}$, TEMPO and $PhCH_3$ were performed using GAUSSIAN 03 or GAUSSIAN 09 software packages[51] and the PBE1PBE functional, without symmetry constraints. This functional uses a hybrid generalized gradient approximation (GGA), including a 25% mixture of Hartree–Fock[52] exchange with DFT[50] exchange correlation, given by the Perdew, Burke, and Ernzerhof functional (PBE).[53] The optimised geometries were obtained with a standard 6-31G(d,p)[54] basis set for all elements (basis b1). The electronic energies obtained were converted to standard free Gibbs energies at 298.15 K by using zero point energy and thermal energy corrections based on structural and vibrational frequency data calculated at the PBE1PBE/b1 level of theory. Single point energy calculations were performed using an improved basis set (basis b2) and the geometries optimised at the PBE1BPE/b1 level. Basis b2 consisted of a standard 6-311++G(d,p).[55] Solvent effects (toluene) were considered in the PBE1BPE/b2//PBE1BPE/b1 energy calculations using the polarizable continuum model (PCM) initially devised by Tomasi and co-workers[56] as implemented in Gaussian 09.[57] The molecular cavity was based on the united atom topological model applied on UAHF radii, optimised for the HF/6-31G(d) level.

## Acknowledgements

The authors thank Fundação para a Ciência e a Tecnologia, Lisbon, Portugal, for funding (SFRH/BPD/73941/2010, SFRH/BPD/79778/2011, PEst-OE/QUI/UI0100/2013, UID/MULTI/00612/2013 and RECI/QEQ-QIN/0189/2012) and the IST-UL Portuguese NMR Network (REM2013, RNNMR).

## References

1 D. Rehder, *Metallomics*, 2015, **7**, 730.
2 D. Rehder, in *Bioinorganic Vanadium Chemistry*, John Wiley & Sons, Ltd, New York, 2008.
3 A. G. J. Ligtenbarg, R. Hage and B. L. Feringa, *Coord. Chem. Rev.*, 2003, **237**, 89.

4 D. C. Crans, J. J. Smee, E. Gaidamauskas and L. Yang, *Chem. Rev.*, 2004, **104**, 849.
5 D. Rehder, *Angew. Chem., Int. Ed. Engl.*, 1991, **30**, 148.
6 R. R. Eady, *Coord. Chem. Rev.*, 2003, **237**, 23.
7 M. R. Maurya, M. Bisht, A. Kumar, M. L. Kuznetsov, F. Avecilla and J. C. Pessoa, *Dalton Trans.*, 2011, **40**, 6968.
8 H. Hosseini-Monfared, R. Bikas and P. Mayer, *Inorg. Chim. Acta*, 2010, **363**, 2574.
9 P. Adão, J. C. Pessoa, R. T. Henriques, M. L. Kuznetsov, F. Avecilla, M. R. Maurya, U. Kumar and I. Correia, *Inorg. Chem.*, 2009, **48**, 3542.
10 D. Rehder, G. Santoni, G. M. Licini, C. Schulzke and B. Meier, *Coord. Chem. Rev.*, 2003, **237**, 53.
11 N. Zwettler, M. E. Judmaier, L. Strohmeier, F. Belaj and N. C. Mösch-Zanetti, *Dalton Trans.*, 2016, **45**, 14549.
12 C. Bolm, *Coord. Chem. Rev.*, 2003, **237**, 245.
13 M. Sutradhar, L. M. D. R. S. Martins, M. F. C. G. da Silva and A. J. L. Pombeiro, *Coord. Chem. Rev.*, 2015, **301–302**, 200.
14 (*a*) S. Azoulay, K. Manabe and S. Kobayashi, *Org. Lett.*, 2005, **7**, 4593; (*b*) Y. Gu, C. Ogawa, J. Kobayashi, Y. Mori and S. Kobayashi, *Angew. Chem., Int. Ed.*, 2006, **45**, 7217; (*c*) M. Boudou, C. Ogawa and S. Kobayashi, *Adv. Synth. Catal.*, 2006, **348**, 2585.
15 H. Hagen, J. Boersma, M. Lutz, A. L. Spek and G. van Koten, *Eur. J. Inorg. Chem.*, 2001, 117.
16 S. Groysman, I. Goldberg, Z. Goldschmidt and M. Kol, *Inorg. Chem.*, 2005, **44**, 5073.
17 C. Lorber, F. Wolff, R. Choukroun and L. Vendier, *Eur. J. Inorg. Chem.*, 2005, 2850.
18 X. D. Feng, X. X. Zhang, Z. N. Wang, J. Song, Y. H. Xing and F. Y. Bai, *New J. Chem.*, 2016, **40**, 1222.
19 Z. Liu and F. C. Anson, *Inorg. Chem.*, 2001, **40**, 1329.
20 S. Barroso, J. Cui, J. M. Carretas, A. Cruz, I. C. Santos, M. T. Duarte, J. P. Telo, N. Marques and A. M. Martins, *Organometallics*, 2009, **28**, 3449.
21 F. Madeira, S. Barroso, S. Namorado, P. M. Reis, B. Royo and A. M. Martins, *Inorg. Chim. Acta*, 2012, **383**, 152.
22 S. Barroso, F. Madeira, M. J. Calhorda, M. J. Ferreira, M. T. Duarte and A. M. Martins, *Inorg. Chem.*, 2013, **52**, 9427.
23 S. Barroso, A. M. Coelho, S. Gómez-Ruiz, M. J. Calhorda, Z. Zizak, G. N. Kaluderovic and A. M. Martins, *Dalton Trans.*, 2014, **43**, 1722.
24 S. Barroso, P. Adão, A. M. Coelho, J. C. Pessoa and A. M. Martins, *J. Mol. Catal. A: Chem.*, 2016, **412**, 107.
25 S. Barroso, P. Adão, F. Madeira, M. T. Duarte, J. C. Pessoa and A. M. Martins, *Inorg. Chem.*, 2010, **49**, 7452.
26 S. Barroso, P. Adão, M. T. Duarte, A. Meetsma, J. C. Pessoa, M. W. Bouwkamp and A. M. Martins, *Eur. J. Inorg. Chem.*, 2011, 4277.
27 E. Y. Tschuva, M. Versano, I. Goldberg, M. Kol, M. Weitman and Z. Goldschmidt, *Inorg. Chem. Commun.*, 1999, **2**, 371.
28 S. Groysman, I. Goldberg, Z. Goldschmidt and M. Kol, *Inorg. Chem.*, 2005, **44**, 5073.
29 J.-M. Rosset, C. Floriani, M. Mazzanti, A. Chiesi-Villa and C. Guastini, *Inorg. Chem.*, 1990, **29**, 3991.
30 F. Wolff, C. Lorber, R. Choukroun and B. Donnadieu, *Eur. J. Inorg. Chem.*, 2004, 2861.
31 Cambridge Structural Database, version 5.37, Nov 2015, dichloride vanadium(IV) complexes with N/O donors, 4 entries. See for instance: (*a*) M. Pasquali, F. Marchetti and C. Floriani, *Inorg. Chem.*, 1979, **18**, 2401; (*b*) H. Schmidt and D. Rehder, *Inorg. Chim. Acta*, 1998, **267**, 229.
32 (*a*) A. Neves, I. Vencato and Y. P. Mascarenhas, *Acta Crystallogr., Sect. C: Cryst. Struct. Commun.*, 1994, **50**, 1417; (*b*) T. K. Praine, T. Weyhermuller, E. Bill, E. Bothe and P. Chaudhuri, *Eur. J. Inorg. Chem.*, 2003, 4299.
33 F. Wolff, C. Lorber, R. Choukroun and B. Donnadieu, *Inorg. Chem.*, 2003, **42**, 7839.
34 (*a*) J. A. Bonadies and C. J. Carrano, *J. Am. Chem. Soc.*, 1986, **108**, 4088; (*b*) X. Li, M. S. Lah and V. L. Pecoraro, *Inorg. Chem.*, 1988, **27**, 4657; (*c*) J. A. Bonadies, W. M. Butler, V. L. Pecoraro and C. J. Carrano, *Inorg. Chem.*, 1987, **26**, 1218.
35 A. F. Cozzolino, D. Tofan, C. C. Cummins, M. Temprado, T. D. Palluccio, E. V. Rybak-Akimova, S. Majumdar, X. Cai, B. Captain and C. D. Hoff, *J. Am. Chem. Soc.*, 2012, **134**, 18252.
36 E. Tsuchida and K. Oyaizu, *Coord. Chem. Rev.*, 2003, **237**, 213.
37 (*a*) H. Mimoun, L. Saussine, E. Daire, M. Postel, J. Fischer and R. Weiss, *J. Am. Chem. Soc.*, 1983, **105**, 3101; (*b*) M. Mad'avorá, M. Sivák, L. Kuchta, J. Marek and J. Benko, *Dalton Trans.*, 2004, 3313; (*c*) S. Nica, A. Pohlmann and W. Plass, *Eur. J. Inorg. Chem.*, 2005, 2032; (*d*) R. Gyepes, S. Pacigová, M. Sivák and J. Tatiersky, *New J. Chem.*, 2009, **33**, 1515; (*e*) M. R. Maurya, N. Chaudhary, F. Avecilla, P. Adão and J. C. Pessoa, *Dalton Trans.*, 2015, **44**, 1211.
38 T. M. Brown, C. J. Cooksey, A. T. Dronsfield and A.-S. Wilkinson, *Appl. Organomet. Chem.*, 1996, **10**, 415.
39 D. Maity, A. Ray, W. S. Sheldrick, H. M. Figge, B. Bandyopadhyay and M. Ali, *Inorg. Chim. Acta*, 2006, **359**, 3197.
40 (*a*) C. Bolm and F. Bienewald, *Angew. Chem., Int. Ed. Engl.*, 1995, **34**, 2640; (*b*) Y. Wu, J. Liu, X. Li and A. S. C. Chan, *Eur. J. Org. Chem.*, 2009, 2607.
41 H. Egami and T. Katsuki, *J. Am. Chem. Soc.*, 2007, **129**, 8940.
42 See for example the following reviews and the references cited therein: (*a*) J. M. Winter and B. S. Moore, *J. Biol. Chem.*, 2009, **284**, 18577; (*b*) A. Butler, *Coord. Chem. Rev.*, 1999, **187**, 17.
43 L. E. Manzer, *Inorg. Synth.*, 1982, **21**, 135.
44 G. M. Sheldrick, *SADABS, Program for Empirical Absorption Correction*, University of Göttingen, Göttingen, Germany, 1996.
45 M. C. Burla, R. Caliandro, M. Camalli, B. Carrozzini, G. L. Cascarano, L. De Caro, C. Giacovazzo, G. Polidori and R. Spagna, *J. Appl. Crystallogr.*, 2005, **38**, 381.
46 L. J. Farrugia, *J. Appl. Crystallogr.*, 1999, **32**, 837.

 

47 (*a*) G. M. Sheldrick, *SHELXL-97 – Programs for Crystal Structure Analysis (Release 97-2)*, Göttingen, Germany, 1998; (*b*) G. M. Sheldrick, *Acta Crystallogr., Sect. A: Fundam. Crystallogr.*, 2008, **64**, 122.

48 M. N. Burnett and C. K. Johnson, ORTEP-III Report ORNL-6895,Oak Ridge National Laboratory, Tennessee, USA, 1996; L. J. Farrugia, *J. Appl. Crystallogr.*, 1997, **30**, 565.

49 C. F. Macrae, P. R. Edgington, P. McCabe, E. Pidcock, G. P. Shields, R. Taylor, M. Towler and J. van de Streek, *J. Appl. Crystallogr.*, 2006, **39**, 453.

50 R. G. Parr and W. Young, in *Density Functional Theory of Atoms and Molecules*, Oxford University Press, New York, 1989.

51 M. J. Frisch, G. W. Trucks, H. B. Schlegel, G. E. Scuseria, M. A. Robb, J. R. Cheeseman, J. A. Montgomery Jr., T. Vreven, K. N. Kudin, J. C. Burant, J. M. Millam, S. S. Iyengar, J. Tomasi, V. Barone, B. Mennucci, M. Cossi, G. Scalmani, N. Rega, G. A. Petersson, H. Nakatsuji, M. Hada, M. Ehara, K. Toyota, R. Fukuda, J. Hasegawa, M. Ishida, T. Nakajima, Y. Honda, O. Kitao, H. Nakai, M. Klene, X. Li, J. E. Knox, H. P. Hratchian, J. B. Cross, C. Adamo, J. Jaramillo, R. Gomperts, R. E. Stratmann, O. Yazyev, A. J. Austin, R. Cammi, C. Pomelli, J. W. Ochterski, P. Y. Ayala, K. Morokuma, G. A. Voth, P. Salvador, J. J. Dannenberg, V. G. Zakrzewski, S. Dapprich, A. D. Daniels, M. C. Strain, O. Farkas, D. K. Malick, A. D. Rabuck, K. Raghavachari, J. B. Foresman, J. V. Ortiz, Q. Cui, A. G. Baboul, S. Clifford, J. Cioslowski, B. B. Stefanov, G. Liu, A. Liashenko, P. Piskorz, I. Komaromi, R. L. Martin, D. J. Fox, T. Keith, M. A. Al-Laham, C. Y. Peng, A. Nanayakkara, M. Challacombe, P. M. W. Gill, B. Johnson, W. Chen, M. W. Wong, C. Gonzalez and J. A. Pople, *Gaussian 03, Revision C.02*, Gaussian, Inc., Wallingford, CT, 2004.

52 W. J. Hehre, L. Radom, P. v. R. Schleyer and J. A. Pople, in *Ab Initio Molecular Orbital Theory*, John Wiley & Sons, New York, 1986.

53 (*a*) J. P. Perdew, K. Burke and M. Ernzerhof, *Phys. Rev. Lett.*, 1997, **78**, 1396; (*b*) J. P. Perdew, *Phys. Rev. B: Condens. Matter*, 1986, **33**, 8822.

54 (*a*) R. Ditchfield, W. J. Hehre and J. A. Pople, *J. Chem. Phys.*, 1971, **54**, 724; (*b*) W. J. Hehre, R. Ditchfield and J. A. Pople, *J. Chem. Phys.*, 1972, **56**, 2257; (*c*) P. C. Hariharan and J. A. Pople, *Mol. Phys.*, 1974, **27**, 209; (*d*) M. S. Gordon, *Chem. Phys. Lett.*, 1980, **76**, 163; (*e*) P. C. Hariharan and J. A. Pople, *Theor. Chim. Acta*, 1973, **28**, 213.

55 (*a*) A. D. McClean and G. S. Chandler, *J. Chem. Phys.*, 1980, **72**, 5639; (*b*) R. Krishnan, J. S. Binkley, R. Seeger and J. A. Pople, *J. Chem. Phys.*, 1980, **72**, 650; (*c*) A. J. H. Wachters, *J. Chem. Phys.*, 1970, **52**, 1033; (*d*) P. J. Hay, *J. Chem. Phys.*, 1977, **66**, 4377; (*e*) K. Raghavachari and G. W. Trucks, *J. Chem. Phys.*, 1989, **91**, 1062; (*f*) R. C. Binning Jr. and L. A. Curtis, *J. Comput. Chem.*, 1990, **11**, 1206; (*g*) M. P. McGrath and L. Radom, *J. Chem. Phys.*, 1991, **94**, 511; (*h*) T. Clark, J. Chandrasekhar, G. W. Spitznagel and P. von R. Scheleyer, *J. Comput. Chem.*, 1983, **4**, 294; (*i*) M. J. Frisch, J. A. Pople and J. S. Binkley, *J. Chem. Phys.*, 1984, **80**, 3265.

56 (*a*) E. Cancès, B. Mennucci and J. Tomasi, *J. Chem. Phys.*, 1997, **107**, 3032; (*b*) M. Cossi, V. Barone, B. Mennucci and J. Tomasi, *Chem. Phys. Lett.*, 1998, **286**, 253; (*c*) B. Mennucci and J. Tomasi, *J. Chem. Phys.*, 1997, **106**, 5151.

57 (*a*) J. Tomasi, B. Mennucci and R. Cammi, *Chem. Rev.*, 2005, **105**, 2999; (*b*) M. Cossi, G. Scalmani, N. Rega and V. Barone, *J. Chem. Phys.*, 2002, **117**, 43.